NANO LETTERS

pubs.acs.org/NanoLett

Letter

Polaritonic Vortices with a Half-Integer Charge

Lin Xiong,[#] Yutao Li,[#] Dorri Halbertal, Michael Sammon, Zhiyuan Sun, Song Liu, James H. Edgar, Tony Low, Michael M. Fogler, Cory R. Dean, Andrew J. Millis, and D. N. Basov*

Cite This: *Nano Lett.* 2021, 21, 9256–9261

Read Online

ACCESS | Metrics & More | Article Recommendations | Supporting Information

ABSTRACT: Topological spin textures are field arrangements that cannot be continuously deformed to a fully polarized state. In particular, merons are topological textures characterized by half-integer topological charge ±1/2 and vortex-like swirling patterns at large distances. Merons have been studied previously in the context of cosmology, fluid dynamics, condensed matter physics and plasmonics. Here, we visualized optical spin angular momentum of phonon polaritons that resembles nanoscale meron spin textures. Phonon polaritons, hybrids of infrared photons and phonons in hexagonal boron nitride, were excited by circularly polarized light incident on a ring-shaped antenna and imaged using infrared near-field techniques. The polariton field reveals a half-integer topological charge determined by the handedness of the incident beam. Our phonon polaritonic platform opens up new pathways to create, control, and visualize topological textures.

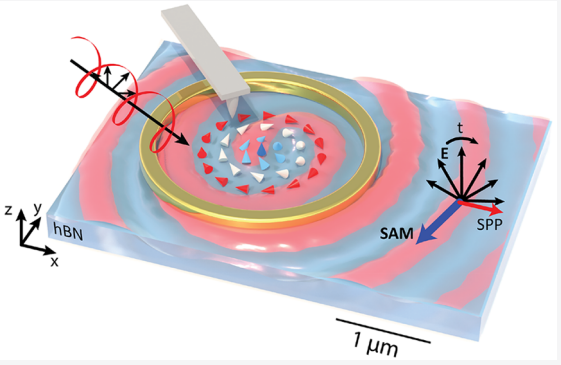

KEYWORDS: *phonon polariton, optical vortex, topology, meron, near-field microscopy*

Topological singularities are commonplace in physical systems such as vortices in superfluids,[1] magnetic topological solitons,[2] and ferroelectric domains.[3] Numerous studies have explored the underlying physical properties of topological textures and their potential applications.[4,5] In condensed matter physics, topological textures manifest themselves as novel spin excitations such as magnetic skyrmions and merons.[6−8] Skyrmions can be thought of as a spatial spin texture covering the full Poincare sphere of polarization, while meron only covers half of the Poincare sphere. Optical analogs of topological spin excitations with integer charge were reported recently in surface plasmons[9−11] and exciton polaritons.[12,13] Here, we study topological textures with a half-integer charge in a fundamentally different system: deeply subdiffractional phonon polariton in a nonmagnetic wide band gap insulator hexagonal boron nitride (hBN). The hBN phonon polaritons[14−18] are hybrids of infrared photons and hBN phonon resonances. Circularly polarized laser beam illuminates a ring-shaped launcher which excites polariton vortex modes propagating in the hBN microcrystals. These polariton vortex modes have an optical phase singularity at the vortex core. Spin angular momentum forms an optical meron texture induced by the spin−orbit interaction of light.[19] The topological charge of the meron excitation is quantized to multiples of half integer. The meron spin texture studied in this work is generic to all confined polaritonic modes,[18] including surface plasmon polaritons of graphene, and waveguide modes of transition metal dichalcogenide.[20] Our platform could help emulating and elucidating the intriguing physics of topological spin excitations via direct nanoimaging experiments.

Analogous to quantum mechanical particles possessing angular momenta, structured optical fields also reveal both orbital angular momentum (OAM) and spin angular momentum (SAM).[21] OAM of light is associated with the optical phase and momentum circulation of the wavefront, such as in an optical vortex beam.[22−25] SAM is an intrinsic property of light which is generated by the vectorial nature of the optical fields.[26−28] A familiar example is that left-handed (LCP) and right-handed circularly polarized light (RCP) admit z-component of SAM $S_z = \pm 1$ respectively,[29] when both waves propagate along the z-direction. Most optical fields possess longitudinal SAM where the optical spin is aligned with the wave propagation directions, and this is associated with an electric field rotating in the transverse plane. In contrast, here we study transverse SAM of phonon polaritons, where SAM is perpendicular to the polariton propagation direction[26,30] (Figure 1a). The surface electric field of phonon polaritons has both transverse (out-of-plane) and longitudinal (along propagation direction) components (Figure 1a). The two

Received: August 16, 2021
Revised: October 18, 2021
Published: October 28, 2021

https://doi.org/10.1021/acs.nanolett.1c03175
Nano Lett. 2021, 21, 9256–9261

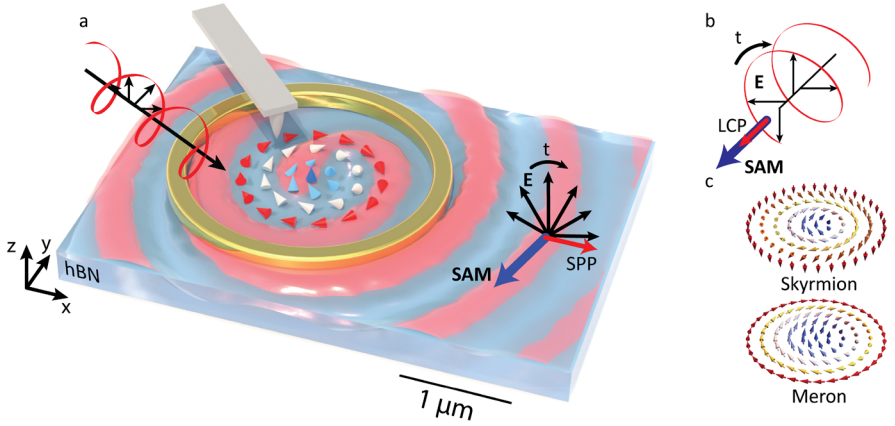

Figure 1. A platform for visualizing spin angular momentum of polaritons. (a) Schematic of a polaritonic vortex generator. Circularly polarized light illuminates the gold ring launcher at 45° incident angle. Spiral polaritons (red shades, representing the intensity of the electric field E_z at a certain time) emanate from the launcher and can be visualized by near-field tip-based imaging techniques. A polaritonic meron spin texture is formed near the vortex core, as represented by colored cones in the interior of the ring launcher. Outside the ring, the time evolution of the polaritonic electric field is depicted by black arrows while the SAM is marked by the blue arrow perpendicular to polariton propagation direction (red arrow). (b) Electric field and SAM direction of a LCP laser beam propagating along the $-y$-direction. For LCP light, the SAM (blue arrow) is aligned with its propagation direction (red arrow). (c) Real-space spin texture of skyrmion and meron quasi-particles. Arrows represent the local spin direction. The polariton SAM texture at the vortex core in panel a resembles the meron spin texture.

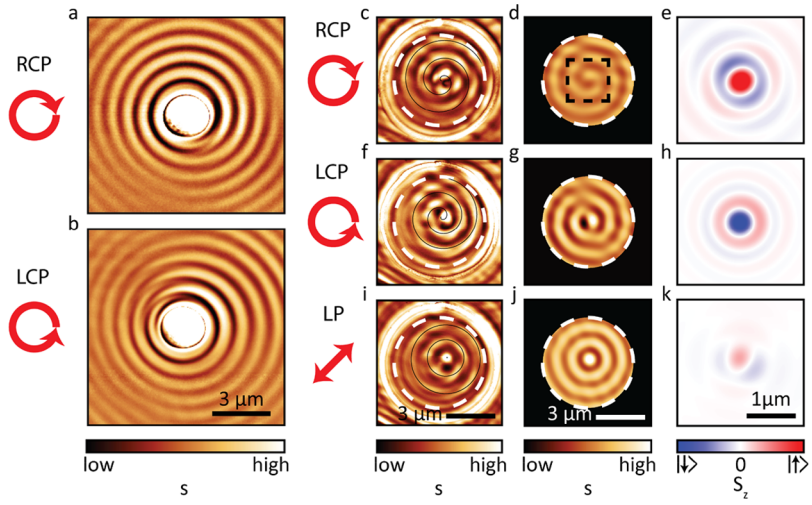

Figure 2. Nanoinfrared images of polaritonic vortexes. (a,b) Near-field images of hBN phonon polaritons excited by a 2 μm diameter disk launcher at laser energy 1490 cm^{-1}. Under the illumination of RCP (panel a) and LCP (panel b) light, polaritons reveal Archimedes spiral fringes. (c) Near-field image acquired at a ring-shaped launcher with RCP incident light, revealing Archimedes spiral fringes. Region used for modeling in panel d is marked with a dashed white circle. The thin black spiral is a guide to the eye. (d) Modeling of experimental results uncovers strong $n = -1$ polariton mode. The dashed square marks the zoomed-in region in panel e. (e) Zoomed-in polariton S_z distribution extracted from the modeling results in panel d, showing a large S_z at the vortex core pointing out of the page. (f–h) same panels as (c–e) illuminated with LCP incident light. Polariton fringes switch chirality and show an anti-Archimedes spiral (panel f). Modeling results reveal dominating $n = +1$ polariton vortex (panel g) with spin pointing into the page at the vortex core (panel h). (i–k) Same panels as c–e illuminated with linearly polarized (LP) light. The polarization direction of the incoming beam is shown by the red arrow. Polariton fringes form concentric circles (panel i). Modeling results show a fringe pattern without any chirality (panel j) and reveal very weak S_z texture (panel k).

components of the electric field have similar magnitude but differ by a 90° phase shift, resulting in a circular rotation of the electric field as a function of time (Figure 1a). One recalls that for circularly polarized light propagating along the $-y$-direction, the electric field vector also rotates in the x–z plane as a function of time, resulting in an optical SAM in the y-direction (Figure 1b). Thus, phonon polaritons possess an intrinsic transverse SAM perpendicular to their propagation direction (blue arrow in Figure 1a) which is referred to as quantum spin Hall effect of light.[19,28] This intuition agrees with the formal definition of SAM for structured optical fields:[26,28]

$$\mathbf{S} = \frac{g}{2}\,\mathrm{Im}(\mathbf{E}^* \times \mathbf{E} + \mathbf{H}^* \times \mathbf{H}) \approx \frac{g}{2}\,\mathrm{Im}(\mathbf{E}^* \times \mathbf{E}) \qquad (1)$$

where $g = (8\pi\omega)^{-1}$ in Gaussian units, and $\mathbf{E}$ and $\mathbf{H}$ are the complex amplitudes of the electric and magnetic fields, respectively. Contributions from magnetic field is negligible for the deeply subdiffractional modes in our experiment. We would like to emphasize that the SAM direction defined in eq 1 is different than the Poincare sphere representation of spin. Numerous theoretical[26,28] and experimental[31] works have explored SAM properties of guided optical modes and utilize SAM to selectively launch optical modes in predefined

https://doi.org/10.1021/acs.nanolett.1c03175
Nano Lett. 2021, 21, 9256–9261

directions.[26,32−35] We built on these works and demonstrated novel SAM textures with half-integer topological charges in phonon polaritons. The topological classification of SAM is obtained by analyzing the distribution of the spin unit vector $\hat{\mathbf{S}} = \mathbf{S}/|\mathbf{S}|$ in a two-dimensional (2D) plane. The topological charge C represents the number of times this unit vector covers the unit sphere as one travels in the plane. Formally, the topological charge density D is given by[7]

$$D = \frac{1}{4\pi}\hat{\mathbf{S}}\cdot(\partial_x\hat{\mathbf{S}} \times \partial_y\hat{\mathbf{S}}) \tag{2}$$

The topological charge C is the integral of D over the plane. For an optical skyrmion,[9,10] SAM swirls from the north pole at the core to the south pole at infinity, encompassing the entire unit sphere once, which yields a topological charge $C = +1$ (Figure 1c). This result is easy to illustrate directly for the case of a rotationally symmetric SAM distribution, where the topological charge density reduces to

$$D(r) = -\frac{1}{4\pi r}\frac{\mathrm{d}\hat{S}_z}{\mathrm{d}r} \tag{3}$$

and the topological charge is given by $C = \frac{1}{2}[\hat{S}_z(0) - \hat{S}_z(\infty)]$. In a meron, spins point out-of-plane at the center,[6,36] $\hat{S}_z(0) = \pm 1$, and are aligned in-plane at infinity, $\hat{S}_z(\infty) = 0$, circulating either clockwise or counterclockwise (Figure 1c). Accordingly, a meron possesses only "half" of a skyrmion's topological charge $C = \pm 1/2$. In a magnetic system, merons are typically stabilized by in-plane magnetic anisotropy.[37−39] Here, we demonstrated an optical meron spin texture induced by the spin−orbit interaction of light[19] in an hBN phonon polariton system. Meron spin texture with topological charge $C = \pm 1/2$ is revealed in Bessel−Gaussian polariton mode with azimuthal number $n = \pm 1$.

We utilized infrared scanning near-field optical microscopy (SNOM) to image the polaritonic vortexes. Our platform (Figure 1a) is comprised of a 70 nm thick hBN slab augmented with gold disk or ring-shaped launchers on top, serving as polaritonic vortex generators. Circularly polarized light at laser energy 1490 cm^{-1} illuminates the launcher and excites polaritonic vortex modes propagating in the hBN slab. It is worth noting that the size of the focused laser spot is the same as the entire field of view in Figure 1a. The rotation symmetry of the launcher implies that the phase of polaritons is solely determined by the handedness of the incoming infrared beam. A tip of an atomic force microscope (AFM) scans on the sample surface and scatters the local electric field into far-field radiation. The tip-scattered light is registered by a detector and the near-field amplitude signal s is extracted by a proper demodulation scheme (Methods).

hBN phonon polaritons excited by a circularly polarized incident beam reveal signatures of spiral polariton fringes (Figure 2). Under RCP illumination, a disk launcher in the middle of the field of view excites clear Archimedes spiral fringes (Figure 2a), in stark contrast to the fringe patterns generated using linearly polarized beam.[40] When switching the incoming beam polarization to LCP, the chirality of the excited spiral fringes is reversed (Figure 2b). These Archimedes spiral fringes are expected to reveal a phase singularity at the center, which motivates us to image polaritons excited by a ring-shaped launcher (Figure 2c,f,i). Under RCP illumination, hBN phonon polaritons excited by the ring-shaped launcher propagate both outward and toward the center of the ring. Nanoimaging data in Figure 2c display an Archimedes spiral fringe and clearly reveal the optical phase singularity at the center (Figure 2a). These Archimedes spiral fringes originate from the interference of waves excited by all sections of the ring-shaped launcher. This uncommon pattern is further confirmed by eigen-mode decomposition modeling (Supporting Information (SI) Note 2). More specifically, the near-field image within the dashed circle is modeled using a superposition of $n = 0$ and ± 1 vortex mode, where n is the azimuthal number of the polaritonic vortex mode. The modeling reveals a dominating $n = -1$ vortex mode (Figure 2d). The diagonal plane wave fringes in the experimental data (Figure 2c) and modeling results (Figure 2d) are induced by a neighboring gold launcher outside of the field of view. Using the modeled near-field image, we inferred the electric field vector $\mathbf{E}$ on the top surface of hBN and calculated the SAM distribution of the polariton vortex mode using procedures detailed in SI Note 2. The electric field $\mathbf{E}$ reveals a phase singularity at the origin while the z-component of the inferred SAM shows a large positive value at the center (Figure 2e). The phase singularity originates from the incident circularly polarized light which induces a winding of the phonon polariton optical phase around the circumference of the ring launcher. Propagating polariton modes carry the winding number toward the center and form the phase singularity. Similar to the electric field pattern of the RCP incident light, the polariton electric field at the center rotates clockwise as a function of time and is confined in a length-scale much smaller than the incoming beam wavelength. One recalls that SAM of RCP light is antialigned with the wave propagation direction. We thereby conclude that the SAM of the incident light is transferred to the polariton modes, leading to a positive S_z at the center of the ring.

When we switch the incoming beam to LCP light, the polariton fringes abide and their chirality is reversed (Figure 2f). The spiraling feature is more apparent once we perform eigen-mode decomposition modeling. The modeled near-field image reveals a dominating $n = +1$ vortex mode (Figure 2g) in contrast to the $n = -1$ vortex seen in the RCP case (Figure 2d). Polariton spin texture inferred from our modeling shows a negative S_z at the center (Figure 2h), coaligned with the incoming beam direction. This is expected as SAM of LCP light is coaligned with the beam propagation direction (Figure 1b) and the SAM is transferred from the incident beam to the polariton mode. When the incident laser beam is linearly polarized (LP), phonon polariton fringes form concentric circles without any chirality (Figure 2i,j) and show very weak spin textures (Figure 2k). Because the linearly polarized incident beam does not carry any SAM, we do not expect SAM to be transferred to polaritons. It is worth noting that linearly polarized beam can excite polariton vortex when coupled with a spiral antenna.[12,41,42]

Zoomed-in view of the extracted polariton SAM distribution reveals the formation of meron-like spin textures (Figure 3). Away from the vortex core, SAM points along the azimuthal direction and circulates clockwise around the vortex core. Moving toward the center, polariton spin gradually switched to radial direction. At the vortex core, SAM points along the out-of-plane z-direction (Figure 3a). The spin texture resembles a topological meron excitation where topological charges are quantized to multiples of 1/2 (Figure 1c). To further examine the observed spin texture, we calculated the topological charge density D (eq 2 and Figure 3b) which is highly concentrated in

https://doi.org/10.1021/acs.nanolett.1c03175
Nano Lett. 2021, 21, 9256−9261

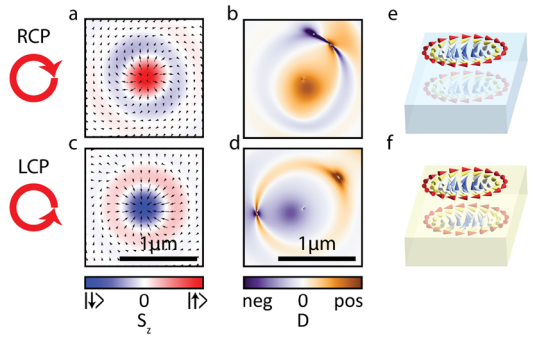

Figure 3. Modeled SAM and topological charges of polariton vortex modes. (a) Zoomed-in view of the extracted polariton SAM induced by RCP light. The arrows represent the in-plane SAM and the false-color map shows the z-component of SAM. S_z is strongly peaked in the center and SAM is largely in-plane away from the vortex core, forming an optical meron excitation. (b) Topological charge density D in the vicinity of the vortex. Topological charge density is strongly concentrated in the center. (c,d) Same as panels a,b measured using LCP light. The SAM in the vortex core (panel c) changes direction compared to panel a and shows strongly negative topological charge density in the center (panel d). (e) Simulated real space spin texture of phonon polariton above and below the hBN surface. The excitation laser energy resides in the hBN upper reststrahlen band. (f) Same as panel e in the case of surface plasmon polaritons. The vorticity of the spin texture is different in opposite sides of the metal surface.

the vortex core where the direction of polariton spin changes rapidly from in-plane to out-of-plane. The integral of topological charge density yields a topological charge of +0.5 within the accuracy of the calculation. For "pure" polariton vortex modes, the topological charge density can be computed from eq 3. In this case, $\hat{S}_z(0) = +1$ and $\hat{S}_z(\infty) = 0$, yielding the topological charge of exactly +0.5. The elliptical distortion of the extracted topological charge density is due to the oblique incident laser beam (SI Note 3). By switching the incoming beam polarization to LCP light, the spin orientation at the vortex core is reversed (Figure 3c). This leads to a reversal of the topological charge density at the center (Figure 3d) and results in a topological charge of −0.5, in accordance with our simulation results.

We remark that the clockwise rotation of spin along the perimeter is largely unaffected by the incoming beam polarization. The directions of these spins are locked with the phonon polariton propagation direction[30] and are not affected by the incoming beam polarization. In the vicinity of the perimeter, polaritons propagate toward the center, and their spin is locked to the azimuthal direction. One may wonder about the case where incident light is some linear combination of LCP and RCP. As the coefficients of this linear combination changes, a sudden transition between topological charges of +0.5 and −0.5 should occur. This transition becomes possible when the electric field develops a singular point in space where the local SAM vector $\mathbf{S}$ vanishes so that the direction of $\hat{\mathbf{S}}$ is undefined.

The polariton vortex modes explored in this work are unique in at least two aspects. First, in the studied range of mid-infrared frequencies ω, hBN behaves as a hyperbolic medium with positive out-of-plane permittivity $\epsilon^z(\omega) > 0$ and negative in-plane permittivity $\epsilon^{//}(\omega) < 0$. As a result, the z-component of the electric field E_z has the same sign above and below the hBN surface, resulting in an identical spin texture on both sides of the hBN surface (Figure 3e). In contrast, for an isotropic metal, which supports surface plasmon polaritons, $\epsilon^z(\omega) = \epsilon^{//}(\omega) < 0$. The sign of E_z changes when crossing the metal surface, leading to a reversal of in plane SAM (Figure 3f). The vorticity of spin texture is opposite on the two sides of the metal surface. Second, the chirality of the polariton modes in our system is easily controlled by incoming beam polarization.

In future experiments, it may be interesting to explore if phonon polariton meron excitations may transfer topological charge to a proximate electronic systems[43,44] or create spin singularities and macroscopic coherent states.[45] The meron excitations may also drive gyroelectric effects and induce on-chip optical nonreciprocity.[46]

METHODS

Near-Field Imaging Techniques. Near-field imaging measurements were performed using a room-temperature scattering-type scanning near-field optical microscope (s-SNOM, Neaspec GmbH).[47] The s-SNOM apparatus is based on a taping mode AFM, coupled to a continuous-wave quantum-cascade laser (Daylight Solution). The incoming laser beam is focused onto the sample using a high-NA off-axis parabolic mirror. The AFM tip is tapped above the sample surface at a frequency of ∼75 kHz. The tip-scattered light is demodulated using a pseudoheterodyne detection scheme[48] to extract both the near-field amplitude $s(\mathbf{r}, \omega)$ and phase $\phi(\mathbf{r}, \omega)$. To properly suppress background contributions to the near-field signal, we demodulate at the fourth harmonic of the tip tapping frequency.

Generation of Mid-Infrared Circularly Polarized Light. The generation of mid-infrared circularly polarized light was achieved using a Fresnel rhomb-based phase retarder. The retarder is composed of two ZnSe rhomboids in series. ZnSe was chosen for its relatively uniform refractive index of 2.4 throughout the mid-IR spectral range. The rhomboids were designed to have a base angle of 51.8°, resulting in a phase retardation of 67.5° between the normal and parallel electric phase components per total internal reflection. Therefore, as the incoming beam passes through the retarder it gains an accumulated phase retardation of 270°, after four total internal reflections. Upon aligning the retarder at an angle of 45° relative to the polarization of the incoming linearly polarized beam, the beam coming out of the retarder would be circularly polarized.

Sample Fabrication. The device consists of five circular metal rings on an hBN flake. The isotopically pure $h^{11}BN$, grown by the metal flux method,[49] is used to achieve longer phonon polariton propagation lengths. $h^{11}BN$ flakes are exfoliated on a SiO_2 substrate from a $h^{11}BN$ crystal by mechanical exfoliation. A polypropylene carbonate (PPC) film attached to a polydimethylsiloxane (PDMS) stamp is used to transfer an $h^{11}BN$ flake of thickness ∼70 nm onto a SiO_2 chip with alignment marks. Ring patterns of widths 150 nm and diameters of 2, 2, 4, 7, and 10 μm are written on the PMMA-coated SiO_2 chip containing the $h^{11}BN$ flake using electron beam lithography. Two nanometers of Cr and 65 nm of Au are then deposited on the chip. Finally, metal lift-off is performed with an acetone soak aided by ∼10 s of ultrasonic sonication.

ASSOCIATED CONTENT

Supporting Information

The Supporting Information is available free of charge at https://pubs.acs.org/doi/10.1021/acs.nanolett.1c03175.

https://doi.org/10.1021/acs.nanolett.1c03175
Nano Lett. 2021, 21, 9256−9261

Additional theoretical analysis on eigen-model decomposition and elliptical distortion; additional discussion on dependence of SAM texture on polariton quality factor (PDF)

AUTHOR INFORMATION

Corresponding Author

D. N. Basov − *Columbia University, New York, New York 10027, United States*; Email: db3056@columbia.edu

Authors

Lin Xiong − *Columbia University, New York, New York 10027, United States*; orcid.org/0000-0003-1616-108X

Yutao Li − *Columbia University, New York, New York 10027, United States*

Dorri Halbertal − *Columbia University, New York, New York 10027, United States*; orcid.org/0000-0002-1665-0724

Michael Sammon − *University of Minnesota, Minneapolis, Minnesota 55455, United States*

Zhiyuan Sun − *Columbia University, New York, New York 10027, United States*

Song Liu − *Kansas State University, Manhattan, New York 66506, United States*

James H. Edgar − *Kansas State University, Manhattan, New York 66506, United States*

Tony Low − *University of Minnesota, Minneapolis, Minnesota 55455, United States*; orcid.org/0000-0002-5759-5899

Michael M. Fogler − *University of California San Diego, La Jolla, California 92093, United States*

Cory R. Dean − *Columbia University, New York, New York 10027, United States*

Andrew J. Millis − *Columbia University, New York, New York 10027, United States; Center for Computational Quantum Physics, The Flatiron Institute, New York, New York 10010, United States*

Complete contact information is available at: https://pubs.acs.org/10.1021/acs.nanolett.1c03175

Author Contributions

[#]L.X. and Y.L. contributed equally to this work.

Notes

The authors declare no competing financial interest.

ACKNOWLEDGMENTS

We thank Prof. Andrei Sirenko for fruitful discussions about the mid-IR retarder. Polaritons research at Columbia University and theoretical work at the University of Minnesota are supported by NSF/EFRI-1741660. The development of the scanning probe instrumentation at Columbia University is supported as part of Programmable Quantum Materials, an Energy Frontier Research Center funded by the U.S. Department of Energy (DOE), Office of Science, Basic Energy Sciences (BES), under award DE-SC0019443. D.N.B. is the Vannevar Bush Faculty Fellow ONR-VB: N00014-19-1-2630. D.N.B. is a Moore Investigator in Quantum Materials EPIQS GBMF9455. M.M.F. acknowledges support by the Office of Naval Research under Grant N000014-18-1-2722. The Flatiron Institute is a Division of the Simons Foundation. Support for hBN crystal growth from the Office of Naval Research, award N00014-20-1-2474, is appreciated.

REFERENCES

(1) Lounasmaa, O. V.; Thuneberg, E. Vortices in Rotating Superfluid 3he. *Proc. Natl. Acad. Sci. U. S. A.* **1999**, *96*, 7760−7767.

(2) Ackerman, P. J.; Smalyukh, I. I. Static Three-Dimensional Topological Solitons in Fluid Chiral Ferromagnets and Colloids. *Nat. Mater.* **2017**, *16* (4), 426−433.

(3) Lin, S. Z.; Wang, X.; Kamiya, Y.; Chern, G. W.; Fan, F.; Fan, D.; Casas, B.; Liu, Y.; Kiryukhin, V.; Zurek, W. H.; Batista, C. D.; Cheong, S. W. Topological Defects as Relics of Emergent Continuous Symmetry and Higgs Condensation of Disorder in Ferroelectrics. *Nat. Phys.* **2014**, *10* (12), 970−977.

(4) Wen, X.-G. Topological Order: From Long-Range Entangled Quantum Matter to a Unified Origin of Light and Electrons. *ISRN Condens. Matter Phys.* **2013**, *2013*, 1−20.

(5) Wang, J.; Zhang, S. C. Topological States of Condensed Matter. *Nat. Mater.* **2017**, *16* (11), 1062−1067.

(6) Yu, X. Z.; Koshibae, W.; Tokunaga, Y.; Shibata, K.; Taguchi, Y.; Nagaosa, N.; Tokura, Y. Transformation between Meron and Skyrmion Topological Spin Textures in a Chiral Magnet. *Nature* **2018**, *564* (7734), 95−98.

(7) Dai, Y.; Zhou, Z.; Ghosh, A.; Mong, R. S. K.; Kubo, A.; Huang, C.-B.; Petek, H. Plasmonic Topological Quasiparticle on the Nanometre and Femtosecond Scales. *Nature* **2020**, *588* (7839), 616−619.

(8) Gao, N.; Je, S. G.; Im, M. Y.; Choi, J. W.; Yang, M.; Li, Q.; Wang, T. Y.; Lee, S.; Han, H. S.; Lee, K. S.; Chao, W.; Hwang, C.; Li, J.; Qiu, Z. Q. Creation and Annihilation of Topological Meron Pairs in In-Plane Magnetized Films. *Nat. Commun.* **2019**, *10* (1), 1−9.

(9) Du, L.; Yang, A.; Zayats, A. V.; Yuan, X. Deep-Subwavelength Features of Photonic Skyrmions in a Confined Electromagnetic Field with Orbital Angular Momentum. *Nat. Phys.* **2019**, *15*, 650−654.

(10) Tsesses, S.; Ostrovsky, E.; Cohen, K.; Gjonaj, B.; Lindner, N. H.; Bartal, G. Optical Skyrmion Lattice in Evanescent Electromagnetic Fields. *Science* **2018**, *361* (6406), 993−996.

(11) Davis, T. J.; Janoschka, D.; Dreher, P.; Frank, B.; Meyer zu Heringdorf, F. J.; Giessen, H. Ultrafast Vector Imaging of Plasmonic Skyrmion Dynamics with Deep Subwavelength Resolution. *Science* **2020**, *368* (6489), eaba6415.

(12) Dall, R.; Fraser, M. D.; Desyatnikov, A. S.; Li, G.; Brodbeck, S.; Kamp, M.; Schneider, C.; Höfling, S.; Ostrovskaya, E. A. Creation of Orbital Angular Momentum States with Chiral Polaritonic Lenses. *Phys. Rev. Lett.* **2014**, *113* (20), 1−6.

(13) Donati, S.; Dominici, L.; Dagvadorj, G.; Ballarini, D.; De Giorgi, M.; Bramati, A.; Gigli, G.; Rubo, Y. G.; Szymańska, M. H.; Sanvitto, D. Twist of Generalized Skyrmions and Spin Vortices in a Polariton Superfluid. *Proc. Natl. Acad. Sci. U. S. A.* **2016**, *113* (52), 14926−14931.

(14) Dai, S.; Fei, Z.; Ma, Q.; Rodin, A. S.; Wagner, M.; McLeod, A. S.; Liu, M. K.; Gannett, W.; Regan, W.; Watanabe, K.; Taniguchi, T.; Thiemens, M.; Dominguez, G.; Castro Neto, A. H.; Zettl, A.; Keilmann, F.; Jarillo-Herrero, P.; Fogler, M. M.; Basov, D. N. Tunable Phonon Polaritons in Atomically Thin van Der Waals Crystals of Boron Nitride. *Science* **2014**, *343* (6175), 1125−1129.

(15) Li, P.; Lewin, M.; Kretinin, A. V.; Caldwell, J. D.; Novoselov, K. S.; Taniguchi, T.; Watanabe, K.; Gaussmann, F.; Taubner, T. Hyperbolic Phonon-Polaritons in Boron Nitride for near-Field Optical Imaging and Focusing. *Nat. Commun.* **2015**, *6* (May), 1−9.

(16) Giles, A. J.; Dai, S.; Vurgaftman, I.; Hoffman, T.; Liu, S.; Lindsay, L.; Ellis, C. T.; Assefa, N.; Chatzakis, I.; Reinecke, T. L.; Tischler, J. G.; Fogler, M. M.; Edgar, J. H.; Basov, D. N.; Caldwell, J. D. Ultralow-Loss Polaritons in Isotopically Pure Boron Nitride. *Nat. Mater.* **2018**, *17* (2), 134−139.

(17) Lee, I. H.; He, M.; Zhang, X.; Luo, Y.; Liu, S.; Edgar, J. H.; Wang, K.; Avouris, P.; Low, T.; Caldwell, J. D.; Oh, S. H. Image Polaritons in Boron Nitride for Extreme Polariton Confinement with Low Losses. *Nat. Commun.* **2020**, *11* (1), 3649.

(18) Basov, D. N.; Asenjo-Garcia, A.; Schuck, P. J.; Zhu, X.; Rubio, A. Polariton Panorama. *Nanophotonics* **2020**, *10* (1), 549−577.

(19) Bliokh, K. Y.; Rodríguez-Fortuño, F. J.; Nori, F.; Zayats, A. V. Spin-Orbit Interactions of Light. *Nat. Photonics* **2015**, *9* (12), 796−808.
(20) Hu, F.; Luan, Y.; Scott, M. E.; Yan, J.; Mandrus, D. G.; Xu, X.; Fei, Z. Imaging Exciton-Polariton Transport in MoSe 2 Waveguides. *Nat. Photonics* **2017**, *11* (6), 356−360.
(21) Andrews, D. L.; Babiker, M. *The Angular Momentum of Light*; Cambridge University Press, 2012.
(22) Karimi, E.; Schulz, S. A.; De Leon, I.; Qassim, H.; Upham, J.; Boyd, R. W. Generating Optical Orbital Angular Momentum at Visible Wavelengths Using a Plasmonic Metasurface. *Light: Sci. Appl.* **2014**, *3* (5), e167.
(23) Ji, Z.; Liu, W.; Krylyuk, S.; Fan, X.; Zhang, Z.; Pan, A.; Feng, L.; Davydov, A.; Agarwal, R. Photocurrent Detection of the Orbital Angular Momentum of Light. *Science* **2020**, *368* (6492), 763−767.
(24) Chimento, P. F.; Alkemade, P. F. A.; 't Hooft, G. W.; Eliel, E. R. Optical Angular Momentum Conversion in a Nanoslit. *Opt. Lett.* **2013**, *38* (19), 3891.
(25) Zambrana-Puyalto, X.; Vidal, X.; Molina-Terriza, G. Angular Momentum-Induced Circular Dichroism in Non-Chiral Nanostructures. *Nat. Commun.* **2014**, *5*, 1−7.
(26) Bliokh, K. Y.; Nori, F. Transverse and Longitudinal Angular Momenta of Light. *Phys. Rep.* **2015**, *592*, 1−38.
(27) He, L.; Li, H.; Li, M. Optomechanical Measurement of Photon Spin Angular Momentum and Optical Torque in Integrated Photonic Devices. *Sci. Adv.* **2016**, *2* (9), e1600485.
(28) Bliokh, K. Y.; Smirnova, D.; Nori, F. Quantum Spin Hall Effect of Light. *Science* **2015**, *348* (6242), 1448−1451.
(29) Fujita, T.; Morimoto, K.; Kiyama, H.; Allison, G.; Larsson, M.; Ludwig, A.; Valentin, S. R.; Wieck, A. D.; Oiwa, A.; Tarucha, S. Angular Momentum Transfer from Photon Polarization to an Electron Spin in a Gate-Defined Quantum Dot. *Nat. Commun.* **2019**, *10* (1), 1−6.
(30) Bliokh, K. Y.; Nori, F. Transverse Spin of a Surface Polariton. *Phys. Rev. A: At., Mol., Opt. Phys.* **2012**, *85*, 61801.
(31) Garcés-Chávez, V.; McGloin, D.; Padgett, M. J.; Dultz, W.; Schmitzer, H.; Dholakia, K. Observation of the Transfer of the Local Angular Momentum Density of a Multiringed Light Beam to an Optically Trapped Particle. *Phys. Rev. Lett.* **2003**, *91* (9), 093602.
(32) Lin, J.; Mueller, J. P. B.; Wang, Q.; Yuan, G.; Antoniou, N.; Yuan, X. C.; Capasso, F. Polarization-Controlled Tunable Directional Coupling of Surface Plasmon Polaritons. *Science* **2013**, *340* (6130), 331−334.
(33) Le Feber, B.; Rotenberg, N.; Kuipers, L. Nanophotonic Control of Circular Dipole Emission. *Nat. Commun.* **2015**, *6* (1), 1−6.
(34) Petersen, J.; Volz, J.; Rauschenbeutel, A. Chiral Nanophotonic Waveguide Interface Based on Spin-Orbit Interaction of Light. *Science* **2014**, *346* (6205), 67−71.
(35) Rodríguez-Fortũno, F. J.; Marino, G.; Ginzburg, P.; O'Connor, D.; Martínez, A.; Wurtz, G. A.; Zayats, A. V. Near-Field Interference for the Unidirectional Excitation of Electromagnetic Guided Modes. *Science* **2013**, *340* (6130), 328−330.
(36) Nych, A.; Fukuda, J. I.; Ognysta, U.; Zumer, S.; Muševic, I. Spontaneous Formation and Dynamics of Half-Skyrmions in a Chiral Liquid-Crystal Film. *Nat. Phys.* **2017**, *13* (12), 1215−1220.
(37) Bera, S.; Mandal, S. S. Theory of the Skyrmion, Meron, Antiskyrmion, and Antimeron in Chiral Magnets. *Phys. Rev. Res.* **2019**, *1*, 33109.
(38) Lu, X.; Fei, R.; Zhu, L.; Yang, L. Meron-like Topological Spin Defects in Monolayer CrCl3. *Nat. Commun.* **2020**, *11* (1), 1−8.
(39) Lin, S. Z.; Saxena, A.; Batista, C. D. Skyrmion Fractionalization and Merons in Chiral Magnets with Easy-Plane Anisotropy. *Phys. Rev. B: Condens. Matter Mater. Phys.* **2015**, *91* (22), 224407.
(40) Dai, S.; Ma, Q.; Yang, Y.; Rosenfeld, J.; Goldflam, M. D.; McLeod, A.; Sun, Z.; Andersen, T. I.; Fei, Z.; Liu, M.; Shao, Y.; Watanabe, K.; Taniguchi, T.; Thiemens, M.; Keilmann, F.; Jarillo-Herrero, P.; Fogler, M. M.; Basov, D. N. Efficiency of Launching Highly Confined Polaritons by Infrared Light Incident on a Hyperbolic Material. *Nano Lett.* **2017**, *17* (9), 5285−5290.
(41) Huang, F.; Jiang, X.; Yuan, H.; Sun, X. Generation of Plasmonic Vortex with Linearly Polarized Light. *Plasmonics* **2017**, *12* (3), 751−757.
(42) Tang, B.; Zhang, B.; Ding, J. Generating a Plasmonic Vortex Field with Arbitrary Topological Charges and Positions by Meta-Nanoslits. *Appl. Opt.* **2019**, *58* (4), 833.
(43) Panas, J.; Irsigler, B.; Zheng, J. H.; Hofstetter, W. Bulk Topological Proximity Effect in Multilayer Systems. *Phys. Rev. B: Condens. Matter Mater. Phys.* **2020**, *102* (7), 075403.
(44) Shoman, T.; Takayama, A.; Sato, T.; Souma, S.; Takahashi, T.; Oguchi, T.; Segawa, K.; Ando, Y. Topological Proximity Effect in a Topological Insulator Hybrid. *Nat. Commun.* **2015**, *6*, 6547.
(45) Trang, C. X.; Shimamura, N.; Nakayama, K.; Souma, S.; Sugawara, K.; Watanabe, I.; Yamauchi, K.; Oguchi, T.; Segawa, K.; Takahashi, T.; Ando, Y.; Sato, T. Conversion of a Conventional Superconductor into a Topological Superconductor by Topological Proximity Effect. *Nat. Commun.* **2020**, *11* (1), 159.
(46) Sounas, D. L.; Alù, A. Non-Reciprocal Photonics Based on Time Modulation. *Nat. Photonics* **2017**, *11* (12), 774−783.
(47) McLeod, A. S.; Van Heumen, E.; Ramirez, J. G.; Wang, S.; Saerbeck, T.; Guenon, S.; Goldflam, M.; Anderegg, L.; Kelly, P.; Mueller, A.; Liu, M. K.; Schuller, I. K.; Basov, D. N. Nanotextured Phase Coexistence in the Correlated Insulator V2O3. *Nat. Phys.* **2017**, *13* (1), 80−86.
(48) Ocelic, N.; Huber, A.; Hillenbrand, R. Pseudoheterodyne Detection for Background-Free near-Field Spectroscopy. *Appl. Phys. Lett.* **2006**, *89* (10), 101124.
(49) Liu, S.; He, R.; Xue, L.; Li, J.; Liu, B.; Edgar, J. H. Single Crystal Growth of Millimeter-Sized Monoisotopic Hexagonal Boron Nitride. *Chem. Mater.* **2018**, *30* (18), 6222−6225.

https://doi.org/10.1021/acs.nanolett.1c03175
Nano Lett. 2021, 21, 9256−9261

Supplementary materials for "polaritonic vortices with a half-integer charge"

Lin Xiong[1]†, Yutao Li[1]†, Dorri Halbertal[1], Michael Sammon[2], Zhiyuan Sun[1], Song Liu[3], James H. Edgar[3], Tony Low[2], Michael M. Fogler[4], Cory R. Dean[1], Andrew J. Millis[1,5], D. N. Basov[1]*

[1]Columbia University, New York, 10027, USA.
[2]University of Minnesota, Minneapolis, 55455, USA.
[3]Kansas State University, Manhattan, 66506, USA.
[4]University of California San Diego, La Jolla, 92093, USA.
[5]Center for Computational Quantum Physics, The Flatiron Institute, New York, 10010, USA.
† These authors contributed equally to this work.
* Corresponding author. Email: db3056@columbia.edu

This file contains:

Supplementary Note 1: Simulation of polariton meron excitation

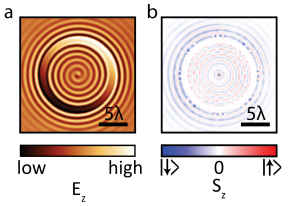

Supplementary Figure 1: FDTD simulation of phonon polaritons excited by gold ring launcher illuminated with circularly polarized light. **a**, Phonon polaritons propagate towards the center of the ring and reveal Archimedes spiral fringes. **b**, Polariton S_z distribution reveals strong negative S_z at the center of the ring.

We employed finite-different time-domain (FDTD) method to simulate phonon polariton propagation. Under the illumination of circularly polarized light, phonon polaritons excited by a gold ring launcher reveals Archimedes spiral fringes (Supplementary Figure 1). Polariton SAM distribution calculated based on eq. 2 reveals clear meron excitation in the center of the ring, with spins pointing down in the vortex core.

Supplementary Note 2: Eigen-mode decomposition and extraction of SAM distribution

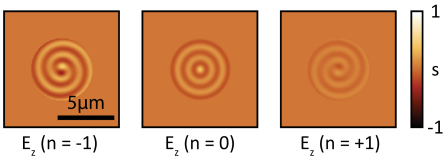

Supplementary Figure 2: Eigen-mode decomposition of experimental data in Fig. 2c into $n = -1$, $n = 0$ and $n = +1$ eigen-modes. $n = -1$ vortex mode has a much larger amplitude compared to other modes. The non-vanishing contribution of the $n = +1$ mode can be attributed to imperfections of the quarter-wave plate and the oblique incident laser beam (Supplementary Note 3). The near-field amplitude is normalized to the maximum value for the $n = -1$ vortex mode.

We model the electric scalar potential at the top surface of hBN as a superposition of eigen-modes of azimuthal angular momentum $n = 0$ and $n = \pm 1$.

$$\psi(r, \varphi) = \sum_{n=0,\pm 1} c_n Z_n(kr) e^{in\varphi}. \tag{S1}$$

Here $k = k_1 + ik_2$ is the in-plane momentum of the polaritons; $Z_n(x)$ is an appropriate Bessel function. Inside the ring, $Z_n(x) = J_n(x)$, the Bessel function of the first kind, which is non-singular at $r = 0$. Outside of the ring $Z_n(x) = H_n^{(1)}(x)$, the Hankel function of the first kind, representing an outgoing wave. The coefficients c_n outside the ring differ from those inside the ring by the factor $J_n(kR)/H_n^{(1)}(kR)$, where R is the radius of the ring. The radial, azimuthal, and z components of the electric field above the hBN surface are $(E_r, E_\varphi, E_z) = -\left(\partial_r, \frac{1}{r}\partial_\varphi, iq_z\right)\psi(r, \varphi)$:

$$(E_r, E_\varphi, E_z) = -\sum_n c_n e^{in\varphi}\left(\partial_r Z_n(kr), \frac{in}{r} Z_n(kr), iq_z Z_n(kr)\right), \tag{S2}$$

where $q_z = ik$ is the out-of-plane momentum. The measured near-field signal corresponds roughly to the z-component. Using Eq. 1 of the main text, the SAM components are found to be

$$S_r = \frac{g}{2r}\,\mathrm{Im}\sum_{n,m} c_m c_n^*\, e^{i(m-n)\varphi}\ (nq_z - mq_z^*) Z_m Z_n^*\,, \tag{S3}$$

$$S_\varphi = \frac{1}{2} g|k|^2\,\mathrm{Im}\sum_{n,m} c_m c_n^*\, e^{i(m-n)\varphi}\ [Z_m (Z_n^*)' - (Z_m)'\, Z_n^*]\,, \tag{S4}$$

$$S_z = \frac{g}{2r}\,\mathrm{Re}\sum_{n,m} c_m c_n^*\, e^{i(m-n)\varphi}[nk(Z_m)'\, Z_n^* + mk^* Z_m (Z_n^*)']\,, \tag{S5}$$

where the derivatives of the Bessel functions are given by the functional identities

$$Z_n'(x) = \frac{n}{x} Z_n(x) - Z_{n+1}(x) = -\frac{n}{x} Z_n(x) + Z_{n-1}(x)\,, \tag{S6}$$

and $Z_m(kr)$ is abbreviated as Z_m.

For "pure" vortices (for which only $n = +1$ or $n = -1$ terms are nonvanishing), the SAM has rotational symmetry. Additionally, if the damping is neglected, $k_2 = 0$, then the SAM inside the ring has only S_r and S_z components. On the other hand, far outside the ring $kr \gg 1$, for any damping, the S_φ component eventually dominates the SAM, giving circulating in-plane SAM texture.

We determined the coefficients c_n by fitting the experimental data. The eigenmode with the largest weight is the dominating mode in the experimental image. To account for the polariton plane waves excited by a neighboring launcher, we also add a plane wave component to the superposition model whose coefficient is also determined by fitting to the experimental image.

Supplementary Note 3: Elliptical distortion of experimental SAM texture

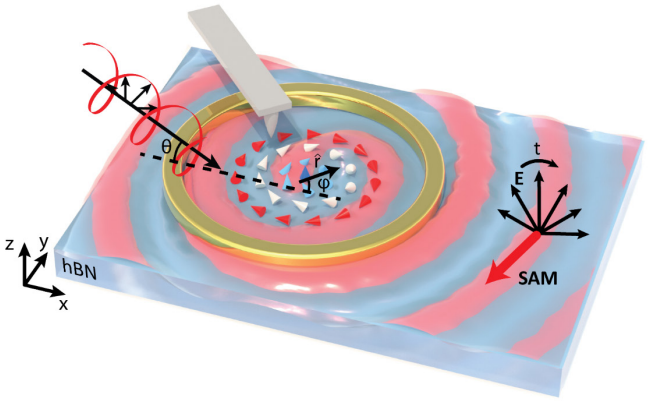

Supplementary Figure 3: Schematic of polariton modes generated by a polaritonic vortex generator. Laser beam incidents at angle θ with respect to the plane. Polariton propagation direction φ is also marked.

Theoretically the SAM distribution induced by circularly polarized incident light should be circularly symmetric. However, the extracted SAM distributions in Fig. 3a and e are elliptically distorted. The origin of this distortion can be traced back to the tilting of the incident beam with respect to normal incidence. This tilting mixes the $n = \pm 1$ modes and results in the observed elliptical distortion. We can quantitatively estimate this mixing by the following argument. For definiteness we assume that the light is incident in the x-z plane with an angle θ with respect to the x axis (Supplementary Figure 3). We suppose that the ring launcher only couples to the component of light that is perpendicular to the ring (i.e. along the radial direction). For the tilted incident beam, we find that the electric field distribution is given by

$$E_r(r, \varphi, z) \propto \hat{\mathrm{r}} \cdot (\sin\theta\,, \pm \mathrm{i}) = \sin\theta \cos\varphi \pm \mathrm{i} \sin\varphi \qquad \text{(S7)}$$

where the $+(-)$ is for RCP (LCP) light. Writing the emitted polariton as a superposition $c_1 E_1 + c_{-1} E_{-1}$ of the $n = \pm 1$ modes, it is straightforward to show that the amplitudes c_1 and c_{-1} are defined by $c_1 + c_{-1} = \sin\theta$ and $c_1 - c_{-1} = \pm 1$. For an incident angle of $\frac{\pi}{6}$, this gives $c_1 = -3c_{-1}$ for RCP light and $c_{-1} = -3c_1$ for LCP light.

Supplementary Note 4: Dependence of SAM texture on polariton quality factor

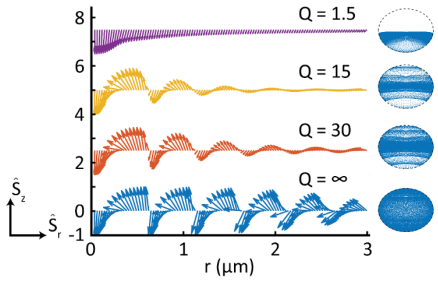

Supplementary Figure 4. Theoretical projection of $\hat{\mathbf{S}}$ onto the $\mathrm{r} - \mathrm{z}$ plane for the region within the ring-shaped launcher for a polariton with topological charge -0.5. We assumed polariton quality factors $Q = 1.5$, $Q = 15$, $Q = 30$ and $Q = \infty$, as indicated in the figure. Line profiles are shifted vertically by multiples of 2.5 for clarity. The corresponding Bloch sphere for each line profiles are shown to the right. As Q decreases, the covering of the Bloch sphere becomes incomplete and the spin angular momentum texture of the inner region becomes more meron-like.

The optical spin texture of polaritons excited by circularly polarized light depends strongly on the polaritonic quality factor Q. We plotted a projection of $\hat{\mathbf{S}}$ onto the r-z plane for the region within the ring-shaped launcher for several different quality factor Q, along with the Bloch sphere representation of the spin distribution in the interior of the launcher (Supplementary Figure 4). For $Q = \infty$, there is substantial SAM oscillation within the r-z plane and a full covering of the Bloch sphere, qualitatively resembling a skyrmion. As Q decreases, the projection of $\hat{\mathbf{S}}$ onto the r-z plane decays exponentially away from the center of the ring. For small enough $Q = 1.5$, the oscillation within this plane is absent, and the SAM texture within the launcher is locked in the azimuthal direction, resembling a meron spin texture. This behavior is in contrast to the region outside of the launcher where polariton spins are aligned along the azimuthal direction.

The different spin texture inside and outside the ring-shaped launcher can be understood in terms of polariton interference. Each piece of the ring-shaped launcher will excite polaritons both towards the center of the ring, and outwards along the radial direction. Due to the screening by the ring itself, the polaritonic waves launched radially outwards cannot interfere with each other, and the SAM is locked in the azimuthal direction. However, the interior region reveals strong interference between polaritonic waves launched from different sections of the ring. The center of the ring has equal interference from all sections of the ring launcher due to symmetry, and results in $\hat{\mathbf{S}}$ being locked along the z-direction. Besides the center of the ring, the polariton interference pattern depends strongly on Q. For high quality samples, this interference can be very strong and results in a skyrmion-like pattern. For low quality samples, the polaritonic wave is almost completely determined by the nearest point of the ring launcher, as all other waves will have exponentially smaller amplitude due to damping effect. This suggests that the SAM texture of the interior region of the launcher can be engineered by the shape of the launcher, the polarization of the light, and the underlying material quality.